Available online at www.sciencedirect.com
ScienceDirect
Materials Chemistry and Physics 106 (2007) 323–329
MATERIALS CHEMISTRY AND PHYSICS
www.elsevier.com/locate/matchemphys

Aqueous gold nanosols stabilized by electrostatic protection generated by X-ray irradiation assisted radical reduction

Chang-Hai Wang [a], Tzu-En Hua [a,b], Chia-Chi Chien [a,c], Yen-Lu Yu [a,d], Tsung-Yeh Yang [a], Chi-Jen Liu [a], Wei-Hua Leng [a], Y. Hwu [a,b,e,*], Yung-Chin Yang [f], Chong-Cook Kim [g], Jung-Ho Je [g], Chih-Hsiung Chen [h], Hong-Ming Lin [i], G. Margaritondo [j]

[a] *Institute of Physics, Academia Sinica, Nankang, Taipei, Taiwan*
[b] *Institute of life science, National Tsing Hua University, Hsinchu, Taiwan*
[c] *Department of Engineering and System Science, National Tsing Hua University, Hsinchu, Taiwan*
[d] *Department of Chemical Engineering, National Taiwan University, Taipei, Taiwan*
[e] *Institute of Opto-Electronics Sciences, National Taiwan Ocean University, Keelung, Taiwan*
[f] *Department of Materials and Mineral Resources Engineering, National Taipei, University of Technology, Taipei, Taiwan*
[g] *Department of Materials Science and Engineering, Pohang University of Science and Technology, Pohang, Republic of Korea*
[h] *Kinsus Interconnect Technology Co., Taoyuang, Taiwan*
[i] *Department of Materials Engineering, Tatung University, Taipei, Taiwan*
[j] *Ecole Polytechnique Fédérate de Lausanne (EPFL), CH-1015 Lausanne, Switzerland*

Received 3 November 2006; received in revised form 8 May 2007; accepted 13 June 2007

Abstract

Reductant, stabilizer-free colloidal gold solutions were fabricated by a new room-temperature synchrotron X-ray irradiation method. The influence of process parameters such as the pH value and the exposure time on the structure of gold nanoparticles was investigated. The mechanisms underlying the X-ray-triggered reduction of gold ions and the formation of gold clusters are discussed in detail. The X-ray irradiation derived highly concentrated gold nanoparticles are readily to be re-dispersed and possess suitable colloidal stability within cellular environment. The characterization included a study of the possible cytotoxicity for the EMT-6 tumor cell line: the negative results indicate that the gold clusters produced with our approach are biocompatible.

Keywords: Gold nanoparticles; X-ray; Synchrotron radiation

1. Introduction

Gold nanoparticles find many applications in science and technology. In medicine, the excellent biocompatibility and high selective agglomeration in cancer cells and tissues [1–3] make them top candidates as drug carriers or radiotherapy enhancers [4]. For biomedical applications, properties such as biocompatibility and dispersion should not be jeopardized by surface modifications or solution conditions.

We present here a new approach meeting these requirements [5], the fabrication of gold nanoparticles by a photosynthesis method using intense X-rays from a synchrotron source. The fabrication process is automatically reductant and stabilizer-free.

The resulting particles were examined by several different techniques revealing in particular their excellent colloidal dispersion and their biocompatibility. The small nanoparticle size is likely to avoid high liver uptake after injection in animals and to result in selective presence in tumors as a consequence of their leaky vasculature [6]. The absence of residue chemical species and the good colloidal stability facilitated our investigations of the interactions between nanoparticles and cells. On the contrary, the commonly used citrate-reduced gold nanoparticles are easily aggregated at high concentration and interfere with the uptake when co-cultured with cells. Alternatively, the citrate groups can be exchanged by other functional ligands that, however, also uncontrollably affect the cell uptake. In both cases, it is difficult

* Corresponding author. Tel.: +886 2 2789 6721; fax: +886 2 2651 0704.
E-mail address: phhwu@sinica.edu.tw (Y. Hwu).

0254-0584/$ – see front matter © 2007 Elsevier B.V. All rights reserved.
doi:10.1016/j.matchemphys.2007.06.024

to study the real uptake mechanisms of high-concentration gold nanoparticles by cellular systems.

In our opinion, unwanted agglomeration is a major obstacle against reliable investigations of the binding, uptake and internalization in biology systems of pure gold nanoparticles—as opposed to coated nanoparticles or nanoparticles coupled to proteins. Our approach, based on irradiation with synchrotron X-rays, provides an effective solution for this problem.

Our method specifically use the X-rays to generate the required electrons in the precursor solutions, whereas the conventional procedure to produce metal particles from bulk ionic solutions requires adding reducing agents to achieve the reduction and supply the electrons. To be successful, our approach needs very intense X-ray beams and, therefore, suitable synchrotron sources. Other procedures based on external stimulation exploited gamma-ray irradiation [7–9], visible laser irradiation [10,11], sonochemical synthesis [12] and microwave heating [13]. However, such methods require stabilizing agents (polymeric molecules) since metallic clusters induced by them tend to coalesce into larger particles. Furthermore, their production rate is rather low: for example, at least 30 h were required for X-ray irradiation with conventional sources [14] and 5 h for gamma-ray irradiation [15] to produce significant amounts of Au nanoparticles.

The production of metallic nanoparticles by X-ray irradiation is not *a priori* obvious because of the much lower energy with respect to gamma-rays. Recent experiments, however, definitely demonstrated the feasibility of this approach [5,14,16–19]. The advantages are clear since the high penetration of X-rays can be exploited to achieve either homogeneous or localized productions in a controlled way. Masking methods can be used to create microscopic patterns. As far nanoparticles quality is concerned, X-ray irradiation offers additional advantages such as cleanliness (the absence of addictives), room-temperature processing, high reproducibility, fast production rate, enhanced biocompatibility and the possibility to reach high nanoparticle concentration. All these factors could be quite relevant to the potential applications in biology, biophysics and biomedicine.

We explored the effects of key process parameters seeking optimal conditions. The underlying physical and chemical mechanisms were analyzed and are discussed later. Extensive characterization of the fabrication products included tests to confirm the high colloidal stability and biocompatibility and to probe the uptake of gold nanoparticles by EMT-6 cells.

2. Experimental

2.1. Materials and methods

Gold nanoparticles were synthesized from aqueous hydrogen tetrachloroaurate trihydrate ($HAuCl_4 \cdot 3H_2O$, Aldrich) solutions by synchrotron X-ray irradiation. Searching for the best irradiation conditions, the pH value of the 1 mM precursor solution (pH 3) was adjusted to 6, 7, 8 and 9 by adding a NaOH solution. We also studied the process for different solution concentrations: 0.5, 1 and 2 mM. The pH value was measured with an Orion 720A pH-meter. Polypropylene conical tubes of different sizes (2, 15 ml, Falcon®, Becton Dickinson, NJ, USA) were used as solution containers. De-ionized water (18.2 MΩ cm, Millipore, Milli-Q, MA, USA) was used throughout the colloidal gold preparation.

The experiments were performed on the 7B2 beamline of 2.5 GeV PLS (Pohang Light Source, Pohang, Korea) and 01A beamline of NSRRC (National Synchrotron Radiation Research Center) storage rings [20]. We used unmonochromatized ("pink") X-ray beams with no optical elements except one set of beryllium and Kepton windows. A slit system was used to obtain a transversal beam section of 3 mm × 9 mm. In addition to a CCD camera installed to monitor the color changes of the solution, the formation of the particles was monitored by synchrotron X-ray microscopy in solution and in real time, specifically analyzing the local change of the metal concentration.

UV and visible light absorption spectra were taken with a UV–vis–NIR spectrometer (spectrometer GBC Cintra 10 e, GBC Scientific. Inc., Australia). The surface charge of gold nanoparticle dispersions were measured by a Malvern Zetasizer 3000 HAS (Malvern Instruments Ltd., Malvern, Worcestershire, UK). The particle morphology, structure and size were measured with a JEOL JEM 2010 F Field Emission Gun Transmission Electron Microscope (FEG-TEM) operating at 200 kV. The samples for TEM measurements were prepared by placing droplets of nanoparticle-containing solution on carbon-coated Cu grids and allowing them to dry.

As-prepared gold nanosols were concentrated by performing centrifugation using centrifuge (Eppendorf® 581OR, Germany) and centrifugal filter device (Amicon® Ultra-15, Milipore, USA). The centrifugation are conducted at 3000 rpm for 20 min under 4 C. To test the re-dispersion capability, highly concentrated gold colloidals (26.2 mg cm^{-3} determined by ICP-OES) were re-dispersed into DI water to reach an optical density above 2. The size and optical absorption of re-dispersed colloidal gold were then examined by dynamic light scatter (DLS) size analyzer (Horiba L-500, Horiba Inc. Japan) and UV–vis spectrometer, respectively.

Gold nanoparticles were also evaluated for their colloidal stability within cellular environment. Aliquots of 0.5 ml of re-dispersed condensed gold nanoparticles (OD > 2) were co-cultured with 0.5 ml of DMEM with 10% serum. The colloidal stability was examined by UV–vis measurement up to 50 h. The variations of three parameters are examined to evaluate the stability of gold particles: (1) peak maximum and (2) full width at half maximum (FWHM) of gold surface plasmon resonance, and (3) integrated area of absorption plot between 550 and 800 nm.

2.2. Cell culture and MTT assay

EMT cells were cultured in DMEM/F12 (GIBCO) medium containing 10% fetal bovine serum (FBS), 1% antibiotics (penicillin at 100 U mL^{-1} and streptomycin at 100 μg mL^{-1}) and L-glutamine at 37 °C in a humidified 5% CO_2 incubator. For MTT assay, MTT reagent (3-[4,5-dimethylthiazol-2-yl]-2,5-diphenyltetrazolium bromide; Thiazolyl blue, Sigma–Aldrich, USA) was dissolved in phosphate buffered saline (PBS, pH 7.4) and filtered through a 0.22 μm filter. EMT-6 cells were seeded within 24-well culture dishes before nanoparticle treatment. After seeding the cells for 24 h, different concentrations of colloidal gold (0, 0.125, 0.25, 0.5, 1, and 2 mM) were added to the microtiter wells. The cells were further incubated for 48 h and then the MTT solution was added to each well to one-tenth the original culture volumes and further incubated for 3–4 h.

Cellular reduction of MTT produces an insoluble, purple formazan. At the end of the incubation period, the formazan crystal was dissolved in dimethyl sulfoxide (DMSO) and the absorbance at 570 nm was measured with a standard microplate reader (Sunrise, Tecan, Switzerland). The quantity of formazan crystal as measured by the amount of absorbance at 570 nm is directly proportional to the number of living cells in culture. Each experiment was performed in triplicate. The relative cell viability (%) was calculated by $([A]_{test}/[A]_{control}) \times 100$, where $[A]_{test}$ is the absorbance of the sample with gold nanoparticles and $[A]_{control}$ is the absorbance of the sample without gold nanoparticles as control.

2.3. TEM analysis

For the TEM sample preparation, 1×10^5 EMT-6 cells were seeded on 100 mm culture dish. After 24 h, concentrated gold colloidals (the volume

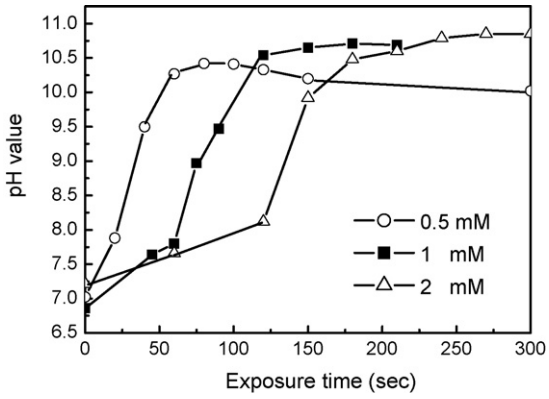

Fig. 1. Variation of the pH value of the X-ray exposed precursor solutions (0.5, 1, 2 mM, 2 ml solution) under continuous X-ray irradiation.

is around 10 μl obtained by centrifuging 3 ml gold nanosol) was added to cells. After co-incubation for 48 h, cells with gold nanoparticles were detached by trypsin (0.5 g porcine trypsin and 0.2 g EDTA·4 NaL^{-1} of Hanks' balanced salt solution) (Sigma, Saint Louis, MO, USA), centrifuged, and washed with PBS for at least three times. Once the trypsin and remnant particles were removed, the cell pellet was fixed with 2.5% glutaraldehyde with 1% tannic acid at 4 °C and retained for 1 h. Then the pellet was washed and post-fixed in 1% Osmium tetroxide for 1 h. The cell pellet then experienced dehydration through a series of ethanol concentrations (30, 50, 70, 80, 90, 95 and 100%). Finally, cell pellets were embedded in resin and sectioned to 90–100 nm in thickness with ultramicrotome (Leica Ultracut R, Leica, Germany) and double stained with uranyl acetate for 20 min and lead citrate for 5 min before the images were taken by JEOL 2010F (JEOL, Japan) operating at 200 kV.

3. Results and discussion

3.1. Formation of colloidal gold under synchrotron X-ray irradiation

The changing pH value of precursor solutions with different concentrations was measured during X-ray irradiation; representative results are shown in Fig. 1. For the three examined concentrations, the pH value increased continuously during the exposure until plateaus were reached. The irradiation time needed to achieve such saturation values increased with the concentration of the precursor solution: 60 s for 0.5 mM, 120 s for 1 mM and 180 s for 2 mM. This evolution was correlated to the kinetic process of gold nanosol formation and will be discussed in detail in the following section.

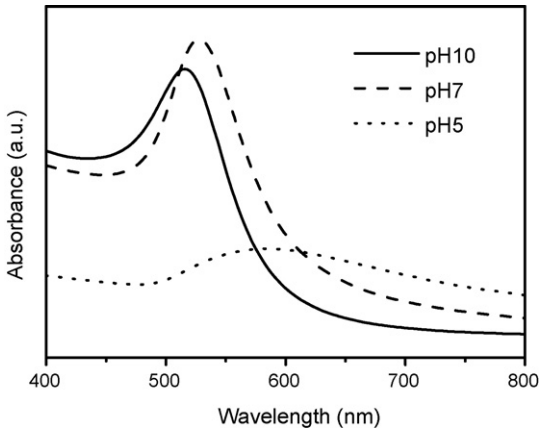

Fig. 3. UV–vis spectra of gold nanosols from precursor solutions with different pH values: (a) 5.3, (b) 7.0 and (c) 10. Exposure time is 5 min for each 10 ml precursor solution.

3.2. Effects of the pH value

We examined the pH value effects on the gold particles size, dispersion and optical absorption properties. TEM Micrographs of gold nanosols obtained from precursor solutions of different pH levels are shown in Fig. 2. The exposure time was set at 5 min for each 10 ml precursor solution. As revealed by Fig. 2(a), under acidic condition the gold particles were strongly flocculated and formed aggregates. The particles obtained from neutral solutions (Fig. 2(b)) did not aggregate and had a size distribution including both large (>20 nm) and small (<10 nm) values. An additional pH increase to 10 (Fig. 2(c)) resulted in the formation of gold nanoparticles with an average size of approximately 10 nm with improved dispersion.

Fig. 3 shows UV–vis absorption spectra of gold solutions for different pH values (5, 7 and 10). The exposure time was also 5 min for each 10 ml precursor solution. The characteristic gold nanoparticle absorption peak due to the surface plasmon resonance [21] was found at 528 nm for pH 7 and at 516 nm for pH 10. For acidic solutions, only a broad peak at 584 nm was observed. This is reasonable since in this case the TEM

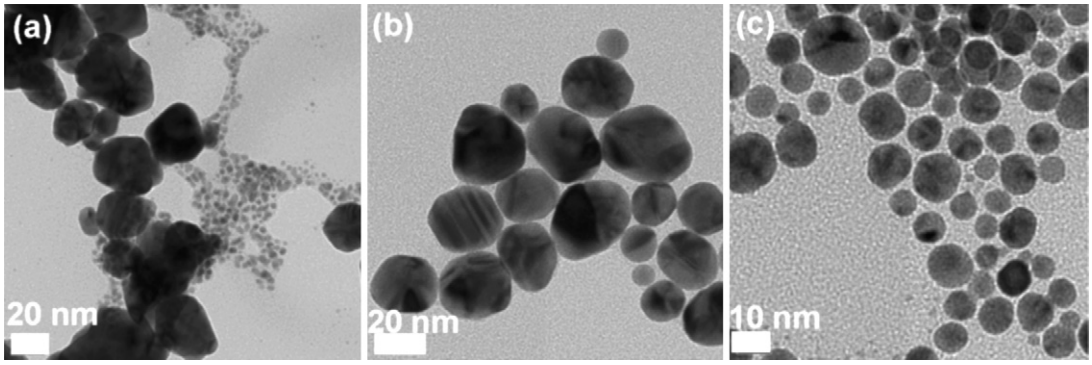

Fig. 2. TEM micrographs of gold nanoparticles from precursor solutions with different pH values: (a) 5.3, (b) 7.0 and (c) 10. Exposure time is 5 min for each 10 ml precursor solution.

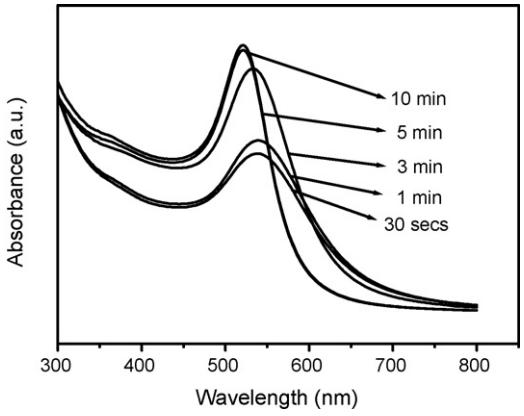

Fig. 4. UV–vis spectra of gold nanosols prepared with different exposure times to the synchrotron X-ray beam. For 10 ml precursor solution.

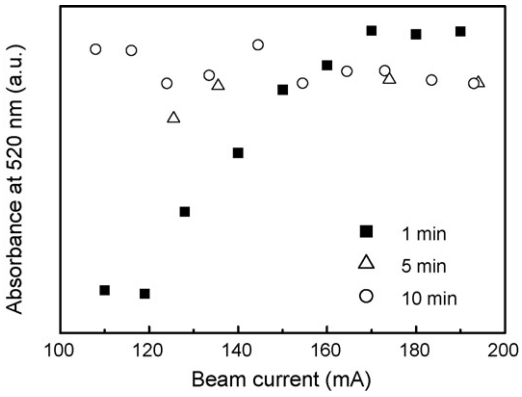

Fig. 5. Variation of absorbance at 520 nm, revealing the amount of gold nanoparticles formed for different electron beam currents in the synchrotron source, corresponding to different X-ray beam intensities.

tests revealed nanoparticle aggregation that results in the disappearance of the characteristic surface plasmon resonance of nanosized particles.

3.3. Effects of the exposure time and of the X-ray beam parameters

Fig. 4 shows the UV–vis spectra of gold nanosols for different exposure times under the conditions of 10 ml precursor solution and 1 mM precursor (pH 10). The surface plasmon resonance shifted towards higher photon energies as the exposure time increased: the peak position was 538, 538, 532, 522 and 520 nm for 30 s, 1, 3, 5 and 15 min—with a parallel decrease of the peak width. Such a shift and peak narrowing indicates a decreasing nanoparticle size.

The natural intensity decrease of the synchrotron source after injection was exploited to investigate the corresponding effects on the nanoparticles formation. Fig. 5 shows the 520 nm surface plasmon resonance peak for different electron beam currents in the synchrotron source (resulting in different X-ray beam intensities). The effects were negligible for exposures longer than 10 min but relevant for shorter times, suggesting that what matters is the total X-ray dose.

3.4. Proposed mechanism for the formation of gold nanoparticle

Free radical $H^{\bullet}$ and $OH^{\bullet}$ are known to develop by dissociation of water molecules exposed to ionization radiation [8,9]. We hypothesize that the active hydrogen-free radical $H^{\bullet}$ acts as an electron donor and the $HAuCl_4$ is reduced to metallic gold through a series of reactions (Eqs. (1)–(4)):

$$HAuCl_4 \rightarrow H^+ + AuCl_4^- \quad (1)$$

$$H_2O \rightarrow H^{\bullet} + OH^{\bullet} \quad (2)$$

$$4OH^{\bullet} \rightarrow 2H_2O + O_2 \quad (3)$$

$$AuCl_4^- + 3H^{\bullet} \rightarrow Au + 3H^+ + 4Cl^- \quad (4)$$

To confirm these steps, the pH value of the bath was measured before and after X-ray irradiation. Table 1 shows, for a solution concentration of 2 mM, the experimental pH values and the theoretical values based on the above equations. We see that before X-ray irradiation the measured pH value of the pure $HAuCl_4$ solution was consistent with the calculated value of the fully ionized $HAuCl_4$ solution. According to Eq. (4), the H^+ concentration should increase three times after complete reaction by X-ray irradiation, and the pH should go down to 2.1. Table 1 also shows results for a $HAuCl_4$ with added NaOH to change the acidity. This is indeed consistent with the measured pH value after the irradiation and confirmed the Au precipitation mechanism (Eqs. (1)–(4)).

According to Eq. (1), the H^+ in solution is due to the $HAuCl_4$ ionization; therefore, a neutral (pH 7) solution should be obtained by neutralizing the H^+ ions with the same concentration of OH, i.e., with a NaOH concentration equal to that of $HAuCl_4$. However, we found that a neutral solution can only be obtained by adding a 4.5 times larger concentration of NaOH. This apparent large discrepancy suggests that NaOH can have other effects besides that of neutralizing the H^+ ions. We also found that the yellow color of the acid $HAuCl_4$ solution progres-

Table 1
The pH value of solutions before and after synchrotron irradiation

Item	Pure $HAuCl_4$ solution		$HAuCl_4$ + NaOH solution	
	Theoretic pH value	Measured pH value	Theoretic pH value	Measured pH value
Before irradiation	2.7	2.69	7	7.08
After irradiation	2.1	2.12	11.3	10.3

Table 2
Re-dispersion capability of highly concentrated pure gold colloidals

Condition	Hydrodynamic size (nm)	Optical density (a.u.)	Gold SPR position (nm)
As synthesized pure gold colloidal	15.5 ± 5.1	1.883	522.7
Re-dispersed concentrated pure gold	17.9 ± 8.9	2.316	521.1

sively changed to colorless with the addition of NaOH. Based on these observations, we propose the following mechanism:

$$AuCl_4^- + 4OH^- \rightarrow Au(OH)_4^- + 4Cl^- \quad (5)$$

$$Au(OH)_4^- + 3H^\bullet \rightarrow Au + 3H_2O + OH^- \quad (6)$$

According to Eqs. (1)–(5), the OH^- replaces the chlorine of $AuCl_4^-$ rather than scavenging the H^+ dissociated from $HAuCl_4$ (Eq. (1)). Therefore, the amount of OH^- required for neutralization by converting all $HAuCl_4$ into $Au(OH)_4^-$ should be five times that of $HAuCl_4$. This is not entirely consistent with the experimental 4.5 times value, indicating that not all the chlorines of $AuCl_4^-$ are replaced by OH^-.

We also found (Table 1) that the pH value increased from 7.08 to 10.3 after synchrotron irradiation. The discrepancy between the experimental and theoretical pH values after irradiation, 10.3 and 11.3, indicates the additional release of OH^- from residual $Au(OH)_4^-$ during the X-ray exposure (Eq. (6)).

Note, indeed, that Au nanoparticles were fabricated with high rate and well dispersed when the pH value was >7. This suggests that the OH^- groups adsorbed on the nanoparticle surfaces causes repulsion between particles and avoids agglomeration. The surface potential of gold nanosols (1 mM) under the condition of pH 9 was -57.8 ± 5 mV as measured using a zeta-meter.

3.5. Re-dispersion capability and colloidal stability

The results of DLS and UV–vis characterization on gold nanoparticle re-dispersion capability are summarized in the Table 2. The size of concentrated colloidal gold after re-buildup in water is largely maintained. The stability in particle size and the absence of agglomeration of re-dispersed colloidal gold were supported by the negligible changes in absorption maximum.

As shown in Fig. 6, the re-dispersed colloidal gold demonstrates sufficient stability in cell culture medium up to 28 h. Additional absorption edges appeared at around 580 nm when further increasing the incubation time. This observation can be contributed to limitation of electrostatic stabilization nature of gold nanoparticles in this study. To achieve better colloidal stability *in vitro* and *in vivo*, steric stabilizing polymers such as polyethylene glycol should be utilized.

3.6. Cytotoxicity and cell uptake tests

Fig. 7 shows the MTT data of colloidal mediated EMT-6 cells continuously assessed for 5 days. We see that the introduction of gold nanoparticle did not affect the mitochondria function and proliferation activities was independent of the Au concentration (up to 2 mM).

Fig. 8 presents the TEM micrographs illustrating the interactions between gold particles and EMT-6 cells. In most observations, the gold nanoparticles were found as clusters and located within the intercellular matrix, as shown in Fig. 8(a). It was also noted that the gold nanoparticles formed larger clusters (Fig. 8(b)) even though individual gold particles can also been differentiated with original size (see inserted image in Fig. 8(b)). Occasionally gold clusters immobilized within cytoplasm can be observed. As described in Fig. 8(c), some gold clusters were internalized while other clusters (arrow marked) were experiencing cellular uptake. The pathway track of internalized gold nanoparticles towards perinuclear region was shown in Fig. 8(d). TEM data indicated that unmodified nanoparticles can penetrate into the EMT-6 cells, even though the amount of cellular uptake is small. This observation is

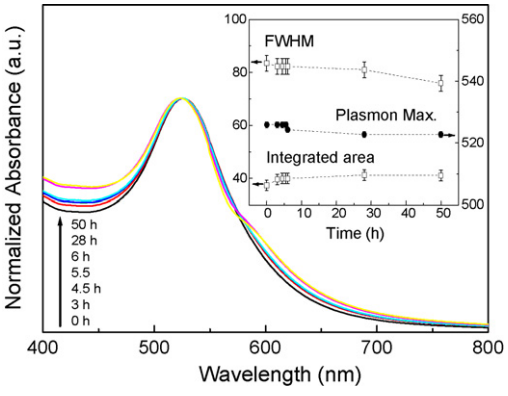

Fig. 6. Colloidal stability of re-dispersed gold colloidals within cell culture medium revealed by UV–vis spectra evolution. The inserted plots describe the variation of the so-called "aggregation markers".

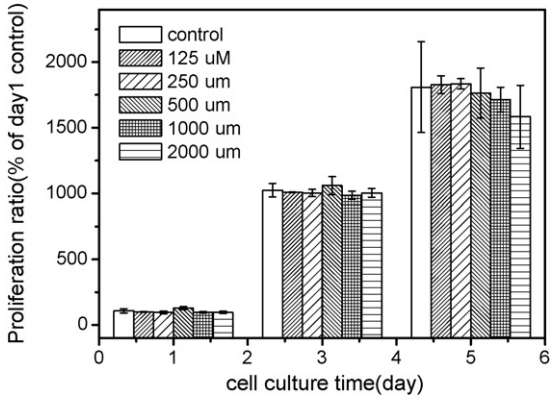

Fig. 7. Dependence of concentration on the viability of colloidal gold particle mediated EMT-6 cells, evaluated by MTT assay.

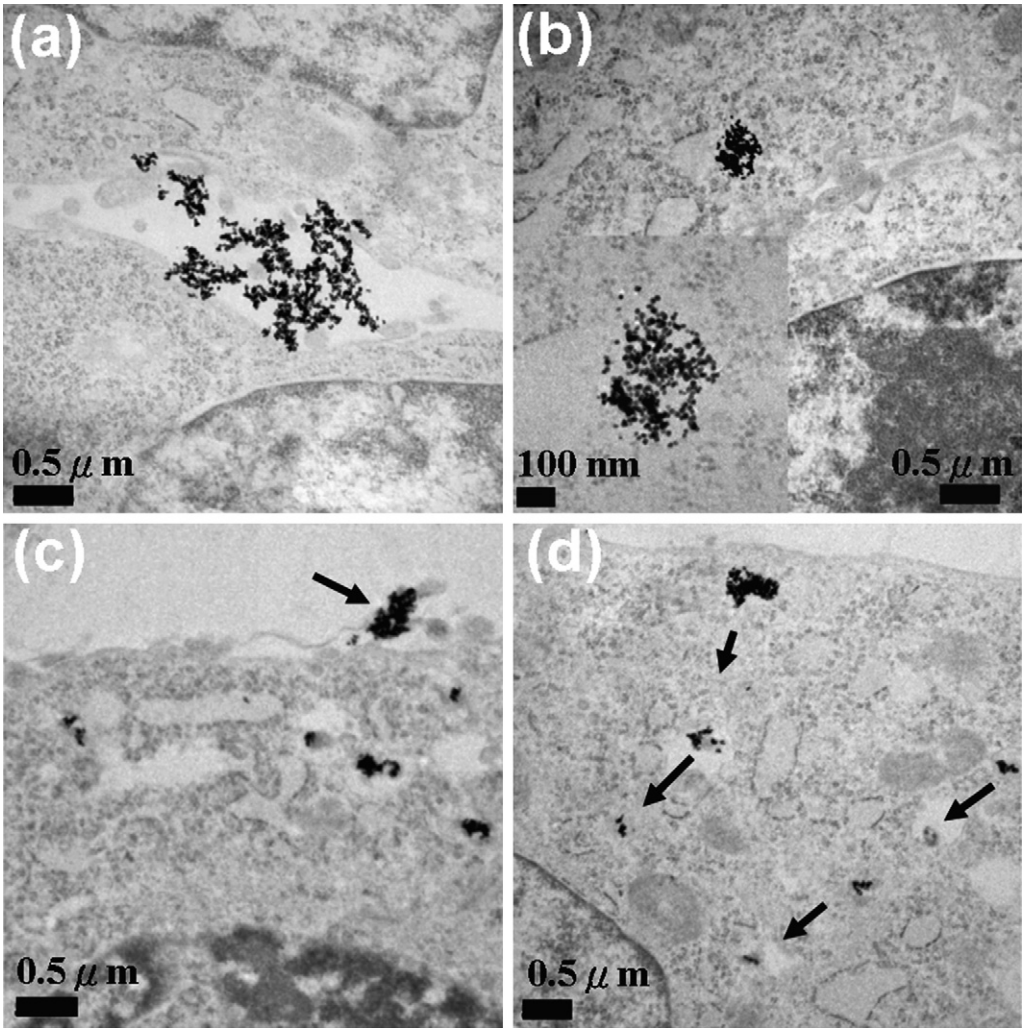

Fig. 8. TEM micrograph depicting the distribution of gold clusters within cellular environments: (a) inter-cellular distribution, (b) cluster of gold nanoparticles, (c) gold nanoparticles attached and uptaken by EMT-6 cell and (d) pathway track of internalized gold nanoparticles towards perinuclear region.

consistent with the aforementioned conclusion that there is no cytotoxicty.

4. Conclusions

We demonstrated that synchrotron X-ray irradiation could produce well-dispersed gold particles (10 nm) in aqueous solutions without adding either a reducing agent or a stabilizer. A mechanism of photo reduction of $HAuCl_4$ and Au nanoparticles formation was proposed based on the experimental results. Gold nanosols prepared with this simple and clean method exhibit good colloidal stability explained by the electrostatic stabilization effect of OH groups. *In vitro* studies indicated that X-ray derived gold nanoparticles don't affect the viability of EMT-6 cells. TEM observation verified that gold nanoparticles can be uptaken by cells.

Acknowledgements

We thank G.M. Chow for the stimulating discussion in characterizing the samples. This work was supported by the National Science Council (Taiwan), by the Academia Sinica (Taiwan), by Creative Research Initiatives (Functional X-ray Imaging) of MOST/KOSEF, by the Swiss Fonds National de la Recherche Scientifique and by the EPFL.

References

[1] R. Shukla, V. Bansal, M. Chaudhary, A. Basu, R.R. Bhonde, M. Sastry, Langmuir 21 (2005) 10644.
[2] G.F. Paciotti, L. Myer, D. Weinreich, D. Goia, N. Pavel, R. Mclaughlin, L. Tamarkin, Drug Deliv. 11 (2004) 169.
[3] J.L. West, N.J. Halas, Curr. Opin. Biotechnol. 11 (2000) 215.
[4] J.F. Hainfeld, D.N. Slatkin, H.M. Smilowitz, Phys. Med. Biol. 49 (2004) N309.
[5] Y.C. Yang, C.H. Wang, Y.K. Hwu, J.H. Je, Mater. Chem. Phys. 100 (2006) 72.
[6] H.F. Dvorak, J.A. Nagy, J.T. Dvorak, A.M. Dvorak, Am. J. Pathol. 133 (1988) 95.
[7] H. Fujita, M. Izawa, H. Yamazaki, Nature 196 (1962) 666.
[8] J. Belloni, M. Mostafavi, H. Remita, J.-L. Marignier, M.-O. Delcourt, New J. Chem. (1998) 1239.
[9] E. Gachard, H. Remita, J. Khatouri, B. Keita, L. Nadjo, J. Belloni, New J. Chem. (1998) 1257.
[10] Z. Geretovszky, T. Szorenyi, Appl. Surf. Sci. 109 (1997) 467.

[11] J.P. Sylvestre, S. Poulin, A.V. Kabashin, E. Sacher, M. Meunier, J.H.T. Luong, J. Phys. Chem. B 108 (2004) 16864.
[12] C.H. Su, P.L. Wu, C.S. Yeh, J. Phys. Chem. B 107 (2003) 14240.
[13] F.K. Liu, C.J. Ker, Y.C. Chang, F.H. Ko, T.C. Chu, B.T. Dai, Jpn. J. Appl. Phys. 42 (2003) 4152.
[14] F. Karadas, G. Ertas, E. Ozkaraoglu, S. Suzer, Langmuir 21 (2005) 437.
[15] A. Henglein, D. Meisel, Langmuir 14 (1998) 7392.
[16] R.A. Rosenberg, Q. Ma, B. Lai, D.C. Mancini, J. Vac. Sci. Technol. B 16 (1998) 3535.
[17] Q. Ma, N. Moldovan, D.C. Mancini, R.A. Rosenberg, Appl. Phys. Lett. 76 (2000) 2014.
[18] H.J. Lee, J.H. Je, Y. Hwu, W.L. Tsai, Nucl. Instr. Method B 199 (2003) 342.
[19] P.H. Borse, J.M. Yi, J.H. Je, W.L. Tsai, Y. Hwu, J. Appl. Phys. 95 (2004) 1166.
[20] S. Baik, H.S. Kim, M.H. Jeong, C.S. Lee, G.H. Je, Y. Hwu, G. Margaritondo, Rev. Sci. Instrum. 75 (2004) 4355.
[21] S. Link, M.A. El-Sayed, J. Phys. Chem. B 103 (1999) 8410.